THE GEOLOGICAL SOCIETY
OF AMERICA®

Effects of secondary phases on crystallographic preferred orientations in mylonites

Andrew J. Cross[1], Greg Hirth[2], and David J. Prior[3]
[1]Department of Earth and Planetary Sciences, Washington University in St. Louis, St. Louis, Missouri 63130, USA
[2]Department of Geological Sciences, Brown University, Providence, Rhode Island 02912, USA
[3]Department of Geology, University of Otago, Dunedin 9056, New Zealand

ABSTRACT

Crystallographic preferred orientations (CPOs) are widely used to infer deformation conditions in the ductile crust and mantle. However, the effects of secondary phases on CPO evolution are not fully understood, despite the compositional diversity of Earth's lithosphere. Here we examine the role of plagioclase on the evolution of quartz CPOs through general shear experiments at 900 °C and 1.1 GPa. Pistons featuring an "asperity" on the shear plane were used, providing a novel way of visualizing CPO evolution under increasing shear strains and with material flow path variations. With the addition of albite, grain boundary pinning inhibits a transition from basal to prism slip, which is observed in single-phase quartz aggregates deformed under the same conditions. Simultaneously, crystallographic axes are modified by rotations around the kinematic vorticity axis, resulting in pronounced weakening of [c]-axis CPOs in the two-phase experiments, where quartz [c]-axes are oriented perpendicular to the vorticity axis. After only modest amounts of deformation (shear strain, γ < 5), CPOs in the single- and two-phase materials become markedly different. These findings highlight complications in using CPOs to infer deformation conditions in well-mixed polymineralic mylonites typical of most lithospheric shear zones.

INTRODUCTION

Crystallographic preferred orientations (CPOs) develop through the rotation and alignment of crystal lattice planes during crystal plastic deformation. Through experimental and field-based studies of single-phase aggregates, CPOs have been shown to vary in strength and symmetry as a function of temperature (Barnhoorn et al., 2004; Law, 2014); stress and water content (Jung et al., 2006); kinematics (Lister and Hobbs, 1980; Boneh and Skemer, 2014); and strain (Barnhoorn et al., 2004; Heilbronner and Tullis, 2006; Hansen et al., 2014). Consequently, CPOs measured in exhumed rocks, or inferred from seismic anisotropy, are commonly used to estimate deformation conditions in the ductile lithosphere. However, given the compositional diversity of Earth's lithosphere, and that well-mixed mineral phases may be required for localized ductile shear (e.g., Bercovici and Ricard, 2012), it is also important to understand the role of secondary phases in modifying CPOs.

It is generally assumed that CPOs are weaker in polyphase rocks, because grain boundary pinning inhibits grain growth and promotes grain size–sensitive (GSS) creep mechanisms (i.e., diffusion creep, grain boundary sliding) that operate at small grain sizes and do not necessarily produce a CPO. Furthermore, grain boundary sliding (GBS) may weaken preexisting CPOs through grain rotations that disperse crystallographic axes (Zhang et al., 1994; Wheeler, 2009) in both polyphase (e.g., Warren and Hirth, 2006; Okudaira and Shigematsu, 2012; Cross and Skemer, 2017) and single-phase rocks (e.g., Jiang et al., 2000; Bestmann and Prior, 2003; Hansen et al., 2011; Miranda et al., 2016; Rahl and Skemer, 2016).

To investigate the influence of secondary phases on CPO evolution, we present microstructural data from deformation experiments on quartz and quartz-albite aggregates. In our experiments, pistons with "asperities" machined on the shear interface were used to produce local thinning of the sample. Because piston displacement is uniform, sample thinning results in spatially-variable finite strains and material flow paths, allowing us to investigate microstructural (e.g., CPO) evolution within a single deformed sample.

EXPERIMENTAL METHODS AND MICROSTRUCTURAL QUANTIFICATION

Aggregates of Black Hills quartz—both with and without 25 vol% Amelia albite—were deformed in a general shear geometry using a Griggs-type apparatus. Quartz and albite powders were sieved to a grain size of <53 µm, mixed together (for the two-phase experiments), dried in a vacuum oven for 24 h, and cold-pressed into an Au jacket between two Al_2O_3 pistons.

Pistons with rigid alumina "asperities" on the shear interface (Fig. 1 inset) were shaped from "green" (unfired) polycrystalline VITA In-Ceram Al_2O_3, using tungsten carbide cutting discs and diamond burrs, before being sintered at 1530 °C for 3.5 h. In addition to standard planar pistons, two types of asperity pistons were used: one with a narrow, semi-cylindrical asperity (1.27 × 0.635 mm in cross section), and one with a wide, tabular asperity (2.54 × 0.635 mm in cross section) (Fig. 1 inset).

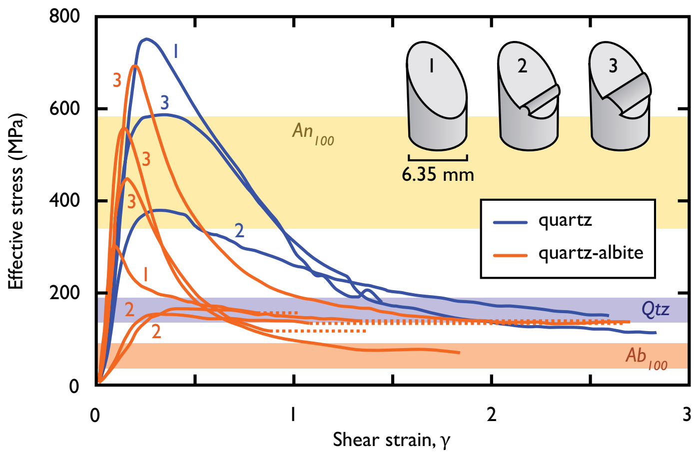

Figure 1. Mechanical data from deformation experiments. Shear strains are those measured in the thickest part of each sample. Effective stress is derived from raw force data, corrected for apparatus compliance but not for changes in the load-supporting area. In some experiments, stress increases due to friction between σ_1 and σ_3 pistons have been removed (dashed lines). Shaded regions correspond to stresses calculated using rheological flow laws for dry quartz (Qtz) (Hirth et al., 2001; Rutter and Brodie, 2004), and dry albite (Ab_{100}) and anorthite (An_{100}) (Rybacki and Dresen, 2004), with a 5 µm grain size and 2.23 GPa water fugacity. Inset: Three-dimensional models of the planar (1), semi-cylindrical (2), and tabular (3) Al_2O_3 pistons used in this study.

Jacketed samples were loaded into a solid-NaCl confining medium cell, then pressurized and heated in a stepwise manner to experimental conditions of 1.1 GPa and 900 °C. After reaching pressure-temperature conditions, the σ_1 piston was advanced rapidly to the hit point (to gauge the location of the sample), retracted 300 µm, and then advanced slowly to deform the sample after achieving a stable cell friction. Deformation occurred at strain rates of $1–1.5 \times 10^{-5}$ in the thicker part of the sample, and a factor of ~2 greater than this in the thinner part of the sample. Finite shear strains are spatially variable (depending on the flow path and therefore the strain history of each grain), but vary between 1 and 6 across each sample. At the end of every experiment, temperatures were rapidly lowered to 300 °C to quench and preserve the microstructure.

Microstructures were analyzed using electron backscatter diffraction (EBSD) mapping of polished sections prepared in the standard reference frame (foliation perpendicular, lineation parallel). Following the methodology outlined in Cross et al. (2015), EBSD maps were processed in the MTEX toolbox for MATLAB (Bachmann et al., 2010), and divided into domains containing at least 500 grains each for quantifying spatial variations in CPO.

SAMPLE STRENGTH AND MICROSTRUCTURES

We deformed three quartz samples and six quartz-albite samples with the different piston types (Table DR1 in the GSA Data Repository[1]). Mechanical data typically show a peak in effective stress, followed by weakening toward a nominal steady-state (Fig. 1). There is no clear relationship between stress magnitude and the piston type used. Weakening in the quartz-albite experiments is more rapid, but all experiments converge to similar stresses (100–200 MPa) at high strains (Fig. 1), coinciding roughly with stresses predicted by rheological flow laws for quartz and albite (Fig. 1). In some experiments, we measured an increase in stress beyond a shear strain of ~1 (Fig. DR1 in the Data Repository). Based on previous experience, we attribute this increase to friction between the σ_1 and σ_3 pistons.

The deformed samples are almost completely recrystallized, particularly in the highest-strain (i.e., thinned) regions. Recrystallized quartz grains are, on average, 3.4 ± 1.7 µm in diameter and slightly elongate, with long axes inclined with respect to the shear plane (Fig. 2). A few large elongate quartz grains are present, containing discrete subgrain boundaries and diffuse intragranular misorientations (Figs. 2A and 2B). Low-angle (2–10°) neighbor-pair misorientation axes cluster in the shear plane, perpendicular to the shear direction (i.e., parallel to the *y* direction; Figs. 2A and 2B insets). In the two-phase experiments, albite microstructures include both long polycrystalline ribbons that pinch and swell, and small (4.1 ± 2.0 µm), fairly equant albite grains that are dispersed throughout the quartz matrix (Figs. 2B and 2C). Intragranular misorientations in albite are small (i.e., on the order of the EBSD angular resolution: 1–2°), suggesting that the polycrystalline albite ribbons formed through the geometric rearrangement of clusters of internally competent grains, most likely by GBS. Overall, our observations suggest that deformation was accommodated primarily through crystal plasticity of quartz, with albite deforming primarily by GSS creep.

CPO EVOLUTION

EBSD data reveal remarkable—and contrasting—evolutions of quartz CPOs in the single- and two-phase experiments (Fig. 3, Figs. DR2 and DR3). Deformation in both the quartz and quartz-albite aggregates initially produces a CPO with quartz [c]-axes inclined slightly from the pole to shear plane (z_{max}), and <a>-axes girdled in a plane inclined antithetically from the shear plane (top left pole figures in Fig. 3, both panels). In the single-phase experiments, quartz [c]-axes rapidly evolve to form a maximum parallel with the vorticity axis (y_{max}), while <a>-axes concomitantly cluster in six maxima within the (x-z) plane normal to the vorticity axis. In contrast, [c]-axes in the two-phase experiments remain clustered around the *z*-direction, and <a>-axes remain girdled near the (x-y) shear plane (right hand pole figures in Fig. 3, lower panel).

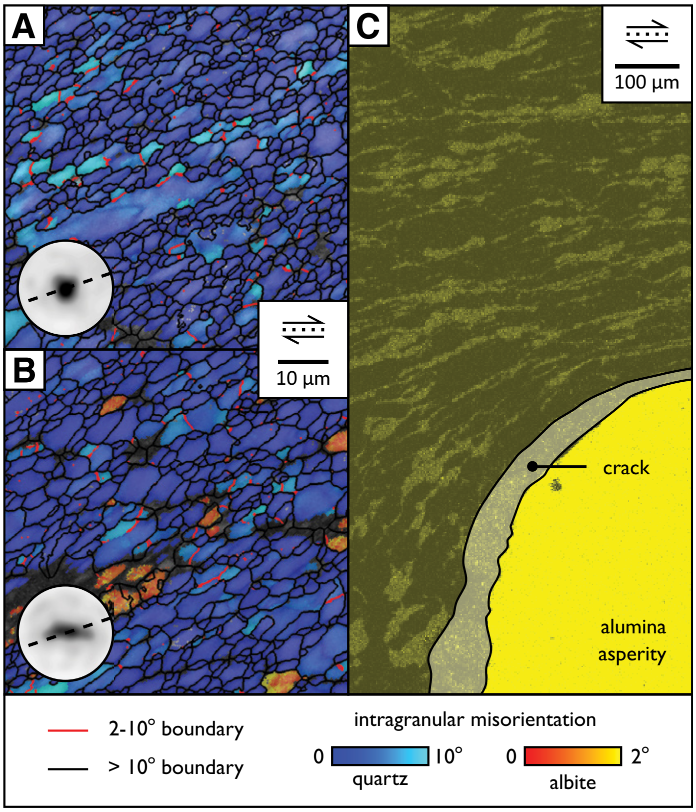

Figure 2. A,B: Electron backscatter diffraction (EBSD) maps (500 nm step size) of quartz (A) and quartz-albite (B) microstructures, collected from high-strain regions (see Fig. 3). Points are colored according to the intragranular misorientation of quartz (blue) and albite (orange) grains, overlain on EBSD band contrast images. Inset: Sample reference frame (equal area, lower hemisphere) contoured stereoplots of neighbor-pair misorientation (2–10°) axes (dashed line represents long axis of local finite strain ellipse). C: Energy-dispersive X-ray spectroscopy (EDS) map of Al content in sample W1921. Light and dark regions correspond to albite and quartz, respectively.

The transition from z_{max} to y_{max} [c]-axis orientations in the single-phase experiments reflects a transition from basal-<a> to prism-<a> dominated slip (see Toy et al., 2008). If facilitated by subgrain rotation (SGR), such a transition would require rotation around an axis parallel with the shear direction (i.e., parallel with the *x*-direction). This is inconsistent with the imposed kinematic reference frame, in which the bulk rotation (vorticity) axis is oriented perpendicular to the shear direction (i.e., parallel with the *y*-direction). Indeed, low-angle neighbor-pair misorientations predominately align parallel with—and therefore imply tilt wall subgrain rotations around—the *y*-direction (Figs. 2A and 2B insets).

A z_{max} to y_{max} transition can also occur by the preferential growth of y_{max}-oriented grains at the expense of z_{max} grains, driven by gradients in intracrystalline strain energy and dislocation density (Muto et al., 2011; c.f Gleason et al., 1993). Our data support this mechanism, since grains can grow freely in the single-phase experiments, whereas grain growth is likely restricted in the two-phase mixtures (e.g., Evans et al., 2001). In other words, albite in the two-phase experiments acts as a pinning phase and largely inhibits the preferential growth of y_{max} grains required for a z_{max} to y_{max} quartz CPO transition.

[1]GSA Data Repository item 2017316, Table DR1 and Figures DR1–DR4, is available online at http://www.geosociety.org/datarepository/2017/ or on request from editing@geosociety.org.

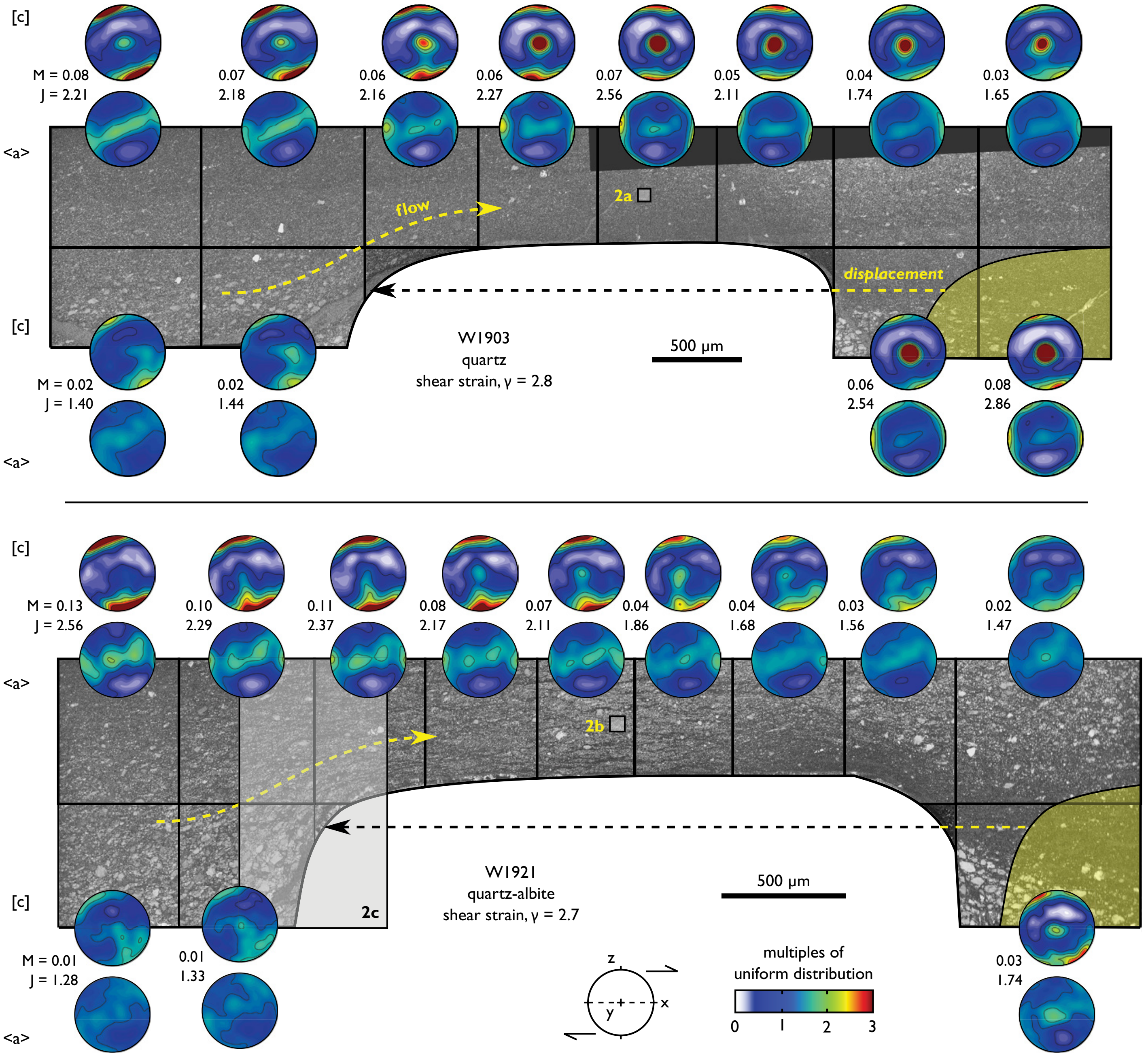

Figure 3. Evolution of quartz [c]- and <a>-axes during shear of quartz (top panel) and quartz-albite (bottom panel) around a tabular piston asperity. Each pole figure (lower hemisphere, equal area) is constructed from one orientation measurement per grain, contoured using a 10° cone half-width, and shown with same intensity scale. Crystallographic preferred orientation (CPO) strengths are given by J- (Bunge, 1982) and M- (Skemer et al., 2005) indices. Background images are electron backscatter diffraction (EBSD) band contrast maps (2 μm step size). Shaded boxes correspond to regions shown in Figure 2. The yellow shaded area shows the initial position of the piston asperity.

With continued flow over the piston asperity, CPO maxima within the *x-z* plane become smeared out, indicating heterogeneous grain rotations around the vorticity axis. This effect is significant in the two-phase samples, where the quartz [c]-axis maximum is perpendicular to the vorticity axis and shear plane, leading to pronounced weakening of the CPO (progressively decreasing J- and M-indices in Fig. 3, lower panel). In the single-phase experiments, however, [c]-axes predominately lie parallel with the vorticity axis and are therefore largely unmodified by the rotation, although the six <a>-axis maxima become smeared out to form a girdle in the *x-z* plane. Because the six <a>-axis maxima are initially oriented 60° apart, their dispersion to form a solid girdle implies grain rotations of ~60° (or more). This rotation does not appear to be caused by flow around the corners of the piston asperities (Fig. DR4) and, in fact, is largely complete before grains exit the thinned part of the sample and pass around the asperity corner (sixth <a>-axis pole figure from top-left in Fig. 3, top panel).

Rotations during plastic deformation primarily result from glide on easy slip planes, SGR, and, if active, GBS. Observations of subgrain boundaries and low-angle misorientations parallel with the vorticity axis (Figs. 2A and 2B) support a role of intracrystalline plastic deformation (i.e., glide, SGR) in dispersing crystallographic axes within the x-z plane. However, the magnitude of grain rotation illustrated by the pole figures (≥60°) is greater than that possible by SGR alone (<20°). We therefore propose that GBS was active in the fine-grained (<10 μm) regions of both the quartz and quartz-albite aggregates, causing further dispersion of the CPO (as in Bestmann and Prior, 2003). It is well known that GBS can operate in polymineralic aggregates due to pinning effects that limit grain growth and promote GSS creep mechanisms (e.g., Warren and Hirth, 2006; Okudaira and Shigematsu, 2012; Cross and Skemer, 2017). However, recent studies have shown that GBS may also operate in single-phase aggregates that have undergone extensive dynamic recrystallization (e.g., Hansen et al., 2011; Miranda et al., 2016; Rahl and Skemer, 2016).

CLOSING REMARKS

Our experiments demonstrate that the presence of secondary phases can significantly modify CPO evolution. After only a modest amount of strain ($\gamma < 5$), CPOs in single- and two-phase samples are markedly different, despite being formed under identical conditions. These findings have implications for the estimation of lithospheric deformation conditions on the basis of CPOs or seismic anisotropy. In quartz-bearing mylonites, for example, y_{max} (prism-<a> dominated slip) CPOs are inferred to form at temperatures of at least 100 °C greater than z_{max} (basal-<a> dominated slip) CPOs (Stipp et al., 2002; Toy et al., 2008). We therefore encourage caution when inferring deformation conditions using CPOs in polymineralic mylonites, particularly where mineral phases are well mixed.

ACKNOWLEDGMENTS

We thank K.C. Li and L. van Rens for producing the pistons used here. Thin sections were prepared by B. Pooley. Experiments W1873 and W1924 were performed by B. Proctor. Comments from R. Heilbronner, S. Mosher, T. Okudaira, J. Rahl, J. Wheeler, and one anonymous reviewer greatly improved the manuscript. This work was supported by a Marsden Fund grant (UOO1116) for Prior, a U.S. National Science Foundation grant (EAR-1220075) for Hirth, and a University of Otago doctoral scholarship for Cross.

REFERENCES CITED

Bachmann, F., Hielscher, R., and Schaeben, H., 2010, Texture analysis with MTEX–free and open source software toolbox: Solid State Phenomena, v. 160, p. 63–68, doi:10.4028/www.scientific.net/SSP.160.63

Barnhoorn, A., Bystricky, M., Burlini, L., and Kunze, K., 2004, The role of recrystallisation on the deformation behaviour of calcite rocks: Large strain torsion experiments on Carrara marble: Journal of Structural Geology, v. 26, p. 885–903, doi:10.1016/j.jsg.2003.11.024.

Bercovici, D., and Ricard, Y., 2012, Mechanisms for the generation of plate tectonics by two-phase grain-damage and pinning: Physics of the Earth and Planetary Interiors, v. 202, p. 27–55, doi:10.1016/j.pepi.2012.05.003.

Bestmann, M., and Prior, D.J., 2003, Intragranular dynamic recrystallization in naturally deformed calcite marble: Diffusion accommodated grain boundary sliding as a result of subgrain rotation recrystallization: Journal of Structural Geology, v. 25, p. 1597–1613, doi:10.1016/S0191-8141(03)00006-3.

Boneh, Y., and Skemer, P., 2014, The effect of deformation history on the evolution of olivine CPO: Earth and Planetary Science Letters, v. 406, p. 213–222, doi:10.1016/j.epsl.2014.09.018.

Bunge, H.J., 1982, Texture Analysis in Materials Science: London, Butterworths, 593 p.

Cross, A.J., and Skemer, P., 2017, Ultramylonite generation via phase mixing in high-strain experiments: Journal of Geophysical Research: Solid Earth, v. 122, p. 1744–1759, doi:10.1002/2016JB013801.

Cross, A.J., Kidder, S., and Prior, D.J., 2015, Using microstructures and TitaniQ thermobarometry of quartz sheared around garnet porphyroclasts to evaluate microstructural evolution and constrain an Alpine Fault Zone geotherm: Journal of Structural Geology, v. 75, p. 17–31, doi:10.1016/j.jsg.2015.02.012.

Evans, B., Renner, J., and Hirth, G., 2001, A few remarks on the kinetics of static grain growth in rocks: International Journal of Earth Sciences, v. 90, p. 88–103, doi:10.1007/s005310000150.

Gleason, G.C., Tullis, J., and Heidelbach, F., 1993, The role of dynamic recrystallization in the development of lattice preferred orientations in experimentally deformed quartz aggregates: Journal of Structural Geology, v. 15, p. 1145–1168, doi:10.1016/0191-8141(93)90161-3.

Hansen, L.N., Zimmerman, M.E., and Kohlstedt, D.L., 2011, Grain boundary sliding in San Carlos olivine: Flow law parameters and crystallographic-preferred orientation: Journal of Geophysical Research, v. 116, B08201, doi:10.1029/2011JB008220.

Hansen, L.N., Zhao, Y.-H., Zimmerman, M.E., and Kohlstedt, D.L., 2014, Protracted fabric evolution in olivine: Implications for the relationship among strain, crystallographic fabric, and seismic anisotropy: Earth and Planetary Science Letters, v. 387, p. 157–168, doi:10.1016/j.epsl.2013.11.009.

Heilbronner, R., and Tullis, J., 2006, Evolution of c axis pole figures and grain size during dynamic recrystallization: Results from experimentally sheared quartzite: Journal of Geophysical Research, v. 111, B10202, doi:10.1029/2005JB004194.

Hirth, G., Teyssier, C., and Dunlap, J.W., 2001, An evaluation of quartzite flow laws based on comparisons between experimentally and naturally deformed rocks: International Journal of Earth Sciences, v. 90, p. 77–87, doi:10.1007/s005310000152.

Jiang, Z., Prior, D.J., and Wheeler, J., 2000, Albite crystallographic preferred orientation and grain misorientation distribution in a low-grade mylonite: Implications for granular flow: Journal of Structural Geology, v. 22, p. 1663–1674, doi:10.1016/S0191-8141(00)00079-1.

Jung, H., Katayama, I., Jiang, Z., Hiraga, T., and Karato, S., 2006, Effect of water and stress on the lattice-preferred orientation of olivine: Tectonophysics, v. 421, p. 1–22, doi:10.1016/j.tecto.2006.02.011.

Law, R.D., 2014, Deformation thermometry based on quartz *c*-axis fabrics and recrystallization microstructures: A review: Journal of Structural Geology, v. 66, p. 129–161, doi:10.1016/j.jsg.2014.05.023.

Lister, G.S., and Hobbs, B.E., 1980, The simulation of fabric development during plastic deformation and its application to quartzite: The influence of deformation history: Journal of Structural Geology, v. 2, p. 355–370, doi:10.1016/0191-8141(80)90023-1.

Miranda, E.A., Hirth, G., and John, B.E., 2016, Microstructural evidence for the transition from dislocation creep to dislocation-accommodated grain boundary sliding in naturally deformed plagioclase: Journal of Structural Geology, v. 92, p. 30–45, doi:10.1016/j.jsg.2016.09.002.

Muto, J., Hirth, G., Heilbronner, R., and Tullis, J., 2011, Plastic anisotropy and fabric evolution in sheared and recrystallized quartz single crystals: Journal of Geophysical Research, v. 116, B02206, doi:10.1029/2010JB007891.

Okudaira, T., and Shigematsu, N., 2012, Estimates of stress and strain rate in mylonites based on the boundary between the fields of grain-size sensitive and insensitive creep: Journal of Geophysical Research. Solid Earth, v. 117, B3, doi:10.1029/2011JB008799.

Rahl, J.M., and Skemer, P., 2016, Microstructural evolution and rheology of quartz in a mid-crustal shear zone: Tectonophysics, v. 680, p. 129–139, doi:10.1016/j.tecto.2016.05.022.

Rutter, E., and Brodie, K., 2004, Experimental intracrystalline plastic flow in hot-pressed synthetic quartzite prepared from Brazilian quartz crystals: Journal of Structural Geology, v. 26, p. 259–270, doi:10.1016/S0191-8141(03)00096-8.

Rybacki, E., and Dresen, G., 2004, Deformation mechanism maps for feldspar rocks: Tectonophysics, v. 382, p. 173–187, doi:10.1016/j.tecto.2004.01.006.

Skemer, P., Katayama, I., Jiang, Z., and Karato, S., 2005, The misorientation index: Development of a new method for calculating the strength of lattice-preferred orientation: Tectonophysics, v. 411, p. 157–167, doi:10.1016/j.tecto.2005.08.023.

Stipp, M., Stünitz, H., Heilbronner, R., and Schmid, S.M., 2002, The eastern Tonale fault zone: A 'natural laboratory' for crystal plastic deformation of quartz over a temperature range from 250 to 700 °C: Journal of Structural Geology, v. 24, p. 1861–1884, doi:10.1016/S0191-8141(02)00035-4.

Toy, V.G., Prior, D.J., and Norris, R.J., 2008, Quartz fabrics in the Alpine Fault mylonites: Influence of pre-existing preferred orientations on fabric development during progressive uplift: Journal of Structural Geology, v. 30, p. 602–621, doi:10.1016/j.jsg.2008.01.001.

Warren, J.M., and Hirth, G., 2006, Grain size sensitive deformation mechanisms in naturally deformed peridotites: Earth and Planetary Science Letters, v. 248, p. 438–450, doi:10.1016/j.epsl.2006.06.006.

Wheeler, J., 2009, The preservation of seismic anisotropy in the Earth's mantle during diffusion creep: Geophysical Journal International, v. 178, p. 1723–1732, doi:10.1111/j.1365-246X.2009.04241.x.

Zhang, Y., Hobbs, B.E., and Jessell, M.W., 1994, The effect of grain-boundary sliding on fabric development in polycrystalline aggregates: Journal of Structural Geology, v. 16, p. 1315–1325, doi:10.1016/0191-8141(94)90072-8.

Manuscript received 4 January 2017
Revised manuscript received 13 July 2017
Manuscript accepted 14 July 2017

Printed in USA